Facile transfer of [2Fe-2S] clusters from the diabetes drug target mitoNEET to an apo-acceptor protein

John A. Zuris[a,1], Yael Harir[b,1], Andrea R. Conlan[a], Maya Shvartsman[b], Dorit Michaeli[b], Sagi Tamir[b], Mark L. Paddock[a], José N. Onuchic[a,2], Ron Mittler[b,c], Zvi Ioav Cabantchik[b], Patricia A. Jennings[a,2], and Rachel Nechushtai[b,2]

[a]Departments of Chemistry and Biochemistry and Physics, University of California at San Diego, La Jolla, CA 92093; [b]The Alexander Silberman Institute of Life Science, Hebrew University of Jerusalem, Edmond J. Safra Campus at Givat Ram, Jerusalem 91904, Israel; [c]Department of Biology, University of North Texas, Denton, TX 76203

Contributed by José N. Onuchic, June 21, 2011 (sent for review May 5, 2011)

MitoNEET (mNT) is an outer mitochondrial membrane target of the thiazolidinedione diabetes drugs with a unique fold and a labile [2Fe-2S] cluster. The rare 1-His and 3-Cys coordination of mNT's [2Fe-2S] leads to cluster lability that is strongly dependent on the presence of the single histidine ligand (His87). These properties of mNT are similar to known [2Fe-2S] shuttle proteins. Here we investigated whether mNT is capable of cluster transfer to acceptor protein(s). Facile [2Fe-2S] cluster transfer is observed between oxidized mNT and apo-ferredoxin (a-Fd) using UV-VIS spectroscopy and native-PAGE, as well as with a mitochondrial iron detection assay in cells. The transfer is unidirectional, proceeds to completion, and occurs with a second-order-reaction rate that is comparable to known iron-sulfur transfer proteins. Mutagenesis of His87 with Cys (H87C) inhibits transfer of the [2Fe-2S] clusters to a-Fd. This inhibition is beyond that expected from increased cluster kinetic stability, as the equivalently stable Lys55 to Glu (K55E) mutation did not inhibit transfer. The H87C mutant also failed to transfer its iron to mitochondria in HEK293 cells. The diabetes drug pioglitazone inhibits iron transfer from WT mNT to mitochondria, indicating that pioglitazone affects a specific property, [2Fe-2S] cluster transfer, in the cellular environment. This finding is interesting in light of the role of iron overload in diabetes. Our findings suggest a likely role for mNT in [2Fe-2S] and/or iron transfer to acceptor proteins and support the idea that pioglitazone's antidiabetic mode of action may, in part, be to inhibit transfer of mNT's [2Fe-2S] cluster.

CISD1 | diabetes | FeS cluster | oxidative stress

MitoNEET (mNT) is a newly discovered target (1) of the insulin-sensitizing thiazolidinedione (TZD) class of type II diabetes drugs (2, 3), which interact with the canonical target PPARγ (4, 5). The interaction of TZD drugs with mNT has been proposed to be of therapeutic importance (1, 6). This is the first iron-sulfur protein to be directly targeted by drug binding (1, 6). The protein contains two [2Fe-2S] clusters, which have been shown to be chemically labile (7). Initial characterization of mNT's redox active and pH labile [2Fe-2S] clusters show that both properties are modulated by binding of TZDs (6, 8), indicating a direct interaction of the protein with the TZD drugs. A second related member of the human NEET protein family, Miner1, is structurally homologous to mNT (9). Miner1 has recently been linked to autophagy, apoptosis, and aging (10, 11), and mis-splicing is associated with a rare disease, known as Wolfram Syndrome 2 (12). Together, mNT and Miner1 represent a new class of NEET iron-sulfur (FeS) proteins characterized structurally by their unique homodimeric fold and rare 3-Cys-1-His [2Fe-2S] cluster ligand environment (6, 9, 13, 14).

Iron-sulfur (FeS) cluster-containing proteins are key players in many essential processes, such as photosynthesis, respiration, and nitrogen fixation (15, 16). They appear in various compositions and confer upon FeS proteins the ability to accept or donate single electrons and/or iron, catalyze enzymatic reactions, or even function as regulatory proteins (17, 18). Disruption of FeS cluster biogenesis is deleterious to vital cell processes in humans, leading to diseases such as Friedreich's ataxia (18, 19), X-linked sideroblastic anemia with ataxia (XLSA/A) (20), and a form of sideroblastic anemia associated with a deletion in the GLRX5 gene (21). The accumulation of iron in mitochondria, which leads to misdistribution of the metal (22) and mismanagement of cellular iron regulatory properties (23, 24), is a hallmark of various diseases. These observations are consistent with the localization of the FeS cluster biogenesis machinery and key FeS protein metabolic functions in mitochondria (16, 23). Moreover, as mitochondria are the primary energy providers of mammalian cells and key players in a large variety of metabolic processes (25), they have been implicated in metabolic diseases such as type II diabetes (26–29).

Human mNT is composed of two protomers intertwined to form a unique structure with two domains; the β-cap and the cluster binding domain and is the founding member of the NEET fold (6, 13, 14, 30). A single-coordinating histidine (H87) along with three cysteine ligands (C72, C74, C83) bind the [2Fe-2S] cluster and the single histidine has been shown to effect cluster redox and stability properties (6–8, 30–33). Our previous studies on the biophysical properties of the protein led us to investigate whether mNT could serve in FeS cluster transfer (6, 7, 31–34). Here we show that mNT transfers its [2Fe-2S] clusters to an apo-acceptor protein. This process occurs only when mNT is in the oxidized state, and mutation of His87 to Cys (H87C) (7, 33) inhibits transfer of the cluster. To assess whether this was a result of the increased cluster stability in the H87C mutant we tested a protein of similar kinetic cluster stability, K55E, and found that it efficiently transfers its [2Fe-2S] cluster to a-Fd. Thus, His87 is critical to efficient cluster transfer. In addition, the transfer rate is orders of magnitude faster than expected from simple release and capture and is quantitative with no apparent loss to degradation that is commonly observed with FeS clusters in solution (16). These results indicate that specific protein–protein interactions between mNT and a-Fd facilitate cluster transfer. As mNT is a target of TZDs we tested its cluster transfer ability in the presence/absence of pioglitazone in permeabilized human embryonic kidney (HEK293) cells. Pioglitazone inhibits transfer suggesting a possible antidiabetic mode of action for the drug under oxidizing conditions.

Results

Oxidized mNT, but Not Reduced, Can Transfer Its [2Fe-2S] Cluster to an Apo-Acceptor Protein. We chose a-Fd for cluster transfer experi-

Author contributions: M.L.P., J.N.O., R.M., Z.I.C., P.A.J., and R.N. designed research; J.A.Z., Y.H., A.R.C., M.S., D.M., and S.T. performed research; J.A.Z., Y.H., A.R.C., M.L.P., J.N.O., R.M., Z.I.C., P.A.J., and R.N. analyzed data; and J.A.Z., Y.H., A.R.C., M.L.P., J.N.O., R.M., Z.I.C., P.A.J., and R.N. wrote the paper.

The authors declare no conflict of interest.

Freely available online through the PNAS open access option.

[1]J.A.Z. and Y.H. contributed equally to this work.

[2]To whom correspondence may be addressed. E-mail: rachel@vms.huji.ac.il or pajennings@ucsd.edu or jonuchic@ucsd.edu.

This article contains supporting information online at www.pnas.org/lookup/suppl/doi:10.1073/pnas.1109986108/-/DCSupplemental.

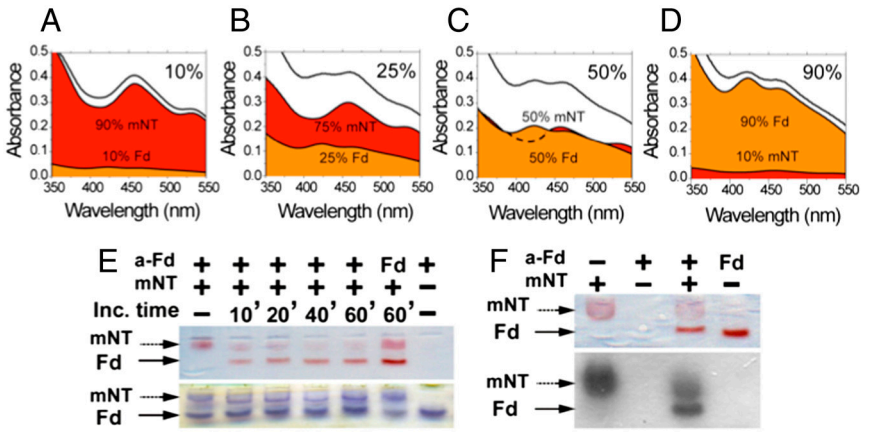

Fig. 1. Facile transfer of the [2Fe-2S] cluster from mitoNEET (mNT) to apo-ferredoxin (a-Fd). The presence of the [2Fe-2S] cluster in mNT can be observed by UV-Vis spectroscopy with a signature peak at 458 nm and in Fd at 423 nm. Frames *A* through *D* show the cluster transfer reaction progress. The observed spectra for the combined species are shown as a black line at the top of each frame while the deconvoluted spectra of holo-mNT (red) and holo-Fd (orange) are shown below. (*D*) Upon approaching completion, the visible spectrum resembles that of Fd, as all a-Fd has been converted to the holo form and mNT has been converted to the visible-lacking apo form. The upper right corner in each spectrum indicates the percent completion for the cluster transfer reaction. (*E*) Transfer of mNT's [2Fe-2S] cluster to a-Fd is also observed by native-PAGE. Upon incubation with a-Fd, mNT shows diminished color, indicating cluster loss over time as the [2Fe-2S] cluster is transferred to a-Fd and the presence of a smaller molecular weight red-colored band indicating formation of holo-Fd. (*F*) In addition, ^{55}Fe-labeled mNT was shown to transfer its cluster to a-Fd by native-PAGE and radioactivity detection. UV-Vis and Native-PAGE cluster transfer experiments were performed at 37 °C using 160 μM a-Fd and 160 μM mNT in the presence of 50 mM Tris pH 8.0, 100 mM NaCl and 5 mM DTT.

ments because (*i*) it is the standard for measuring [2Fe-2S] cluster transfer kinetics and (*ii*) we could take advantage of the fact that Fd has a different ligand environment (4-Cys) than mNT (3-Cys-1-His), leading to a distinguishably different UV-Vis spectrum from which the transfer of mNT's [2Fe-2S] cluster to a-Fd could be easily followed. The UV-Vis spectra of the [2Fe-2S] cluster being transferred changes over time upon mixing of prereduced a-Fd and oxidized mNT under oxidizing conditions as it switches its ligand environment. Deconvolution of the overall spectra show the reaction at 10%, 25%, 50%, and 90% completion (Fig. 1 *A–D*, respectively). These percentages are directly measured from ratio of the peak intensities at 423 nm (Fd) and 458 nm (mNT). Based on initial concentrations of mNT and the final concentration of Fd, we conclude that the [2Fe-2S] cluster transfer was complete and suffers no appreciable loss to solution. This finding was corroborated by native gel electrophoresis (Fig. 1 *E* and *F*, *Upper*), followed by colorimetric and ^{55}Fe-labeled [2Fe-2S] detection (Fig. 1*F*, *Lower*). Holo-mNT's red-colored band intensity decreased over time when incubated with a-Fd, and the latter is concomitantly converted to the red-colored holo-Fd band. The levels of mNT and a-Fd/Fd remained unchanged as shown by Coomassie staining (Fig. 1*E*, *Lower*).

UV-Vis-monitored cluster transfer experiments show that transfer readily occurs under oxidizing conditions as both the initial mNT spectra (Fig. 1*A*) and final Fd spectra (Fig. 1*D*) reflect those of each of the respective oxidized species. As mNT's cluster binding domain on the outer mitochondrial membrane faces the cytosol (7), we wanted to see if transfer was inhibited under reducing conditions like those normally found in this cellular environment. Because both oxidized and reduced mNT have distinct spectra both from each other and Fd we could follow transfer both under oxidizing as well as reducing conditions. Reduced mNT shows no cluster transfer to a-Fd over a period of 500 min (Fig. S1*A*). Upon addition of oxygen mNT becomes oxidized, as seen by the characteristic oxidized spectra (Fig. S1*B*) and readily transfers its [2Fe-2S] cluster to a-Fd (Fig. 2). These results show that mNT's oxidation state regulates whether it can transfer its cluster to a-Fd, and that this cluster transfer capability may normally be inhibited in the reduced cytosolic environment.

His87 Is Critical for Cluster Transfer Between mNT and a-Fd. A projection of mNT's cluster binding site shows the rare 3-Cys-1-His ligand environment around each of the [2Fe-2S] clusters in mNT (Fig. 3*A*). We replaced the coordinating His87 with Cys (H87C) to test the role of this residue in cluster transfer. In addition, we replaced Lys55 with Glu (K55E) because this change dramatically alters the properties of the cluster (31).

Time-dependent spectroscopic changes measured by UV-Vis absorption spectroscopy allowed us to quantitatively measure the rate of cluster transfer for WT mNT and the K55E and H87C mutants. Cluster transfer is slowed only slightly in the K55E mutant whereas the transfer rate was significantly retarded by replacement of the single-coordinating His87 with Cys (Fig. 3 *B* and *C* and Table 1). The transfer rates are distinct from passive decay because (*i*) the transfer rate to a-Fd is concentration dependent, whereas passive decay is not (Fig. S2 *A* and *B*), and (*ii*) the transfer rate is many orders of magnitude faster than passive cluster release (Table 1), hence the reaction is catalyzed. We observed no correlation between kinetic cluster stability and cluster transfer rate because the K55E shows transfer rates similar to WT mNT

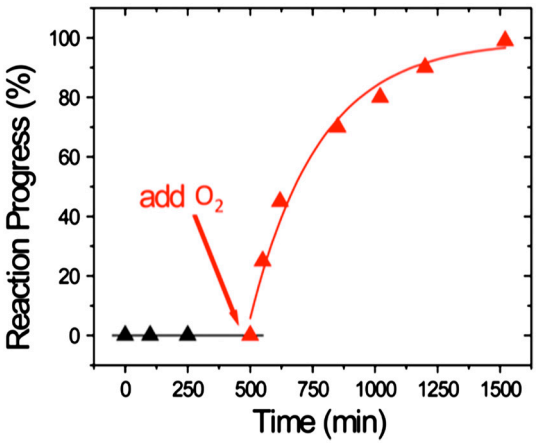

Fig. 2. Facile cluster transfer from mNT to a-Fd occurs only under oxidizing conditions. No reaction progress (i.e., changes in visible spectrum) occurs even after 500 minutes under reducing conditions (black triangles). Upon addition of oxygen to reaction the visible absorption spectrum shifts to that of oxidized mNT (red triangles) and cluster transfer is observed over time. UV-Vis kinetic trace was obtained at 37 °C using 80 μM a-Fd and 80 μM mNT in the presence of 50 mM Tris pH 8.0, 100 mM NaCl and 50 mM DTT.

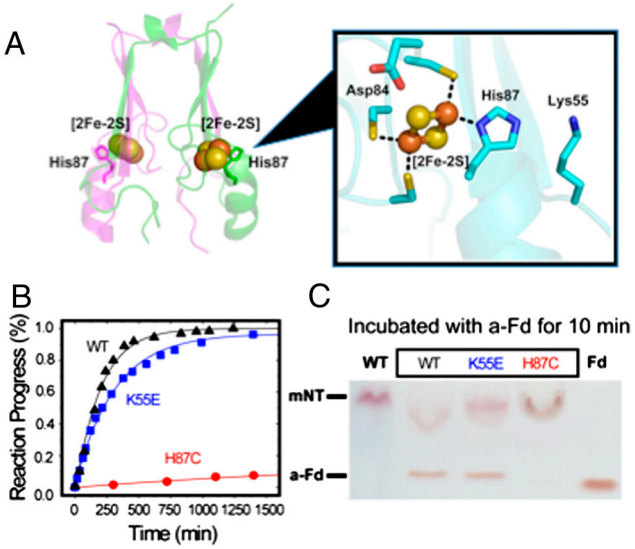

Fig. 3. (*A*) Each [2Fe-2S] cluster in mNT is ligated by 3-Cys-1-His. Enlargement of the cluster binding site shows directly coordinating Cys and His ligands as well as additional local residues that may play key role in cluster transfer. (*B*) UV-Vis absorption spectroscopy kinetics were used to monitor transfer of the [2Fe-2S] in mNT and two mutants: K55E and H87C, to a-Fd. Cluster transfer remains relatively unchanged in the K55E but significantly hindered in the H87C mutant. The cluster transfer reaction for WT mNT (black triangles) shows 50% completion ($A_{423}/A_{458} = 0.5$) in 120 min, the K55E mutant (blue squares) requires 220 min, and the H87C (red circles) requires >10,000 minutes. UV-Vis experiments were performed at 37 °C using 80 μM mNT, 80 μM a-Fd (incubated in 5 mM DTT for 30 min prior to use) in the presence of 50 mM Tris pH 8.0, 100 mM NaCl, and 5 mM EDTA. (*C*) WT mNT and mutant proteins (160 μM, higher protein concentrations are needed for visualization) were incubated with a-Fd for 10 min under similar conditions, followed by native-PAGE. The red-colored upper bands indicate WT mNT and mutant proteins while the lower red bands indicate presence of holo Fd, bearing the [2Fe-2S] cluster from mNT. The results indicate His87 is critical for cluster transfer to an a-Fd acceptor.

(Table 1), yet its kinetic cluster stability is similar to that of the H87C mutant (Table 1 and Fig. S3). The observed cluster transfer rate for mitoNEET is protein concentration dependent with a measured rate constant of 185 ± 11 M^{-1} min^{-1}, a rate constant similar to the well-characterized FeS assembly/transfer protein ISA (170 M^{-1} min^{-1}, Table 1) (35).

The Diabetes Drug Pioglitazone Inhibits Iron Transfer from mNT to Mitochondria. Having demonstrated that mNT can transfer its [2Fe-2S] cluster to an apo-acceptor, we asked if it could be a source of free iron in cells. We used cytosolic and mitochondrial fluorescent indicators to assess changes in free iron levels upon introduction of mNT. We used gently permeabilized HEK293 cells that were double labeled with the fluorescent iron sensors calcein-green (CALG) as tracer for the cytosolic iron, and red rhodamine B-[(1,10-phenanthrolin-5-yl)-aminocarbonyl] benzyl ester (RPA) as a tracer for iron in the mitochondrial matrix (Fig. 4*A*). The changes in fluorescence in response to the addition of mNT are shown in Fig. 4*B*. Quenching of RPA, but not CALG, occurred rapidly and was directly proportional to mNT's concentration (Fig. 4*C*) indicating transfer of iron to the mitochondrial matrix. Preincubation of mNT with a-Fd prevented iron transfer into mitochondria (Fig. 4*D*). We tested the importance of increased cluster stability introduced by mutation or drug binding to iron transfer in the cellular system. The K55E mutant is equivalent to the wild type for iron transfer to the mitochondria whereas H87C mutant inhibits transfer (Fig. 5*A*). Importantly, the addition of pioglitazone to WT inhibited iron transfer (Fig. 5*B*), indicating a PPARγ-independent effect of TZDs.

Table 1. Comparison of mNT cluster transfer rates with mutants and ISA

	Cluster decay half-time (min^{-1})	Initial transfer rate (M^{-1} min^{-1})	Transfer rate at 160 μM [mNT] (min^{-1})	Catalytic enhancement of transfer rate at 160 μM [mNT] (lower limit)
WT	10^{-5}	185 ± 11	0.03	3×10^3
K55E	10^{-6}	115 ± 4	0.02	10^4
H87C	10^{-6}	<1	NA	NA
ISA	NA	170 ± 8*	NA	NA

*Experiment performed at 25 °C on iron-sulfur cluster assembly protein (abbreviated as IscA or ISA) (35).

Discussion

The rare 3-Cys-1-His ligation geometry of the [2Fe-2S] cluster of mNT (6, 13, 36, 37) is only observed in a few other cases, notably in a mutant version of the FeS cluster transfer protein IscU (38), and because the role of IscU is important in FeS cluster assembly we investigated whether mNT can perform cluster transfer. In order to assess this hypothesis, we examined the cluster transfer potential of mNT using a-Fd, a universal acceptor protein used in FeS studies (35). We demonstrate that mNT's [2Fe-2S] cluster is transferable to a-Fd (Fig. 1 *A–F*) at a rate constant (185 ± 11 M^{-1} min^{-1}) equivalent to the cluster transfer protein ISA (170 ± 8 M^{-1} min^{-1}) (35). In addition, we find that replacement of the single His ligand to Cys inhibits the process, emphasizing the importance of this coordination in efficient transfer.

We also show that increased levels of mNT lead to Fe accumulation in mitochondria as reported by RPA fluorescent quenching assays in HEK293 cells (Fig. 5*A*). Fe accumulation is observed with the K55E mutant but not with the H87C mutant protein. Because K55E and H87C have similar cluster stabilities it is clear from this data that His87 is an essential mediator of cluster transfer in cells. The fact that Fe accumulates in the mitochondrial matrix suggests there is a means by which mNT, tethered to the outer mitochondrial membrane, transfers Fe into the matrix. The mechanism in vivo is currently under investigation. Taken together, our findings in the cellular system, which are similar to that observed in vitro, underscore the fact that the conserved His87 ligand facilitates transfer.

TZD cross-linking studies led to the discovery of the mitochondrial target, mNT (1). This target is completely distinct from the accepted paradigm protein, the nuclear transcription factor PPARγ. Here, we report the direct effect of TZD binding to mNT in cellular systems. We show that pioglitazone is capable of regulating Fe accumulation in mitochondria in this study. In addition to providing a cellular readout for TZD binding, this data provides a direct link between previous in vitro observations (6, 8) and our current in vitro and cellular findings. We now present a model describing a possible therapeutic mode of action for pioglitazone (Fig. 6). Because the cytosol is normally highly reducing (39), mNT would be expected to be predominantly in the reduced state. Changes to the cytosolic redox potential, which occur when cells are under oxidative stress (40), could induce transfer of mNT's [2Fe-2S] cluster. If not carefully regulated, this could lead to Fe overload stress, which is a problem in patients with type II diabetes (41). Pioglitazone, which shows a strong preferential binding to mNT in the oxidized state (8), may act to alleviate this stress.

Conclusions and Future Directions

We show that oxidized mNT transfers [2Fe-2S] clusters readily and efficiently, and that reduction of the cluster inhibits transfer. In addition, we show that the hallmark His87 ligand is a critical player in facilitating cluster transfer and provide direct evidence for a functional effect of TZD binding to this protein in cells. Our findings raise a set of interesting questions about this class of

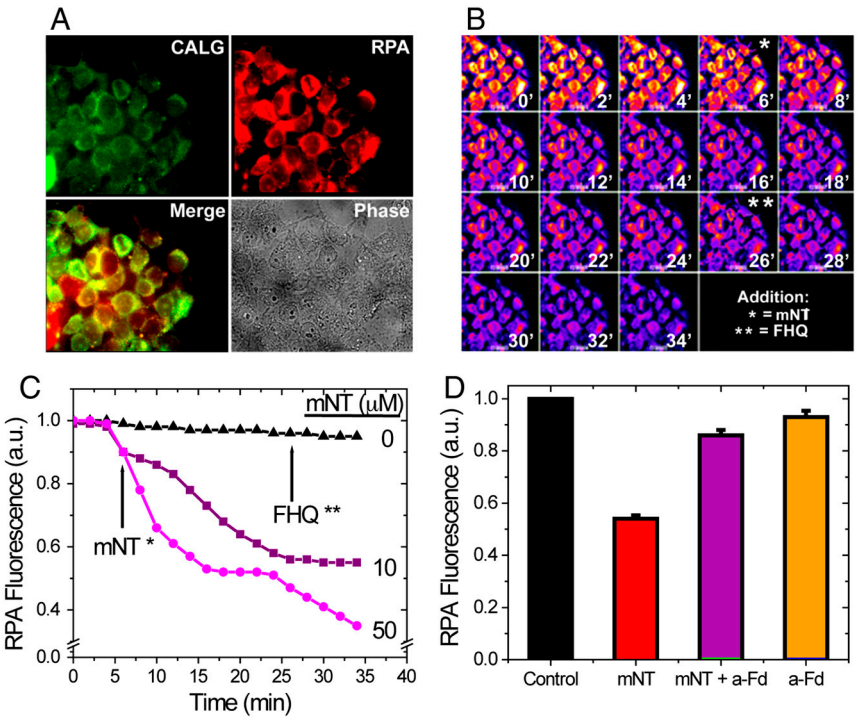

Fig. 4. Transfer of [2Fe-2S]/Fe from mNT to mitochondria in permeabilized HEK293 cells. HEK293 cells labeled with iron sensors RPA (for mitochondria) and calcein-green (CALG) (for cytosol) were permeabilized (*A*) and used for tracing changes in fluorescence by fluorescence microscopy imaging (*B* and *C*) following addition of mNT in succinate medium. (*B*) A time series of fluorescence [pseudocolor images; RPA fluorescence intensity is given in arbitrary units (a.u.)] following addition of 50 μM mNT and FHQ (6 μM) at different times (indicated by * or ** respectively). (*C*) The fluorescence traces (reported as a.u.) represent time series taken for cells exposed to different concentrations of mNT. (*D*) RPA fluorescence 20 minutes after the addition of 10 μM mNT under different conditions. The black bar represents a fluorescence trace from control cells where no additions were made. The red bar represents the fluorescence of cells after mNT addition, the purple bar shows the addition of mNT. In this experiment a-Fd is pretreated with DTT to reduce the free cysteines and prevent inter-disulfides. After 30 min the free DTT is depleted at which point mNT is added. The orange bar represents the fluorescence of cells after addition of a-Fd only. All data are represented as mean ± standard error (SE). The statistical differences between treatments were determined by the paired *t* test at significance levels * $p < 0.05$ or ** $p < 0.01$. ($N = 14$).

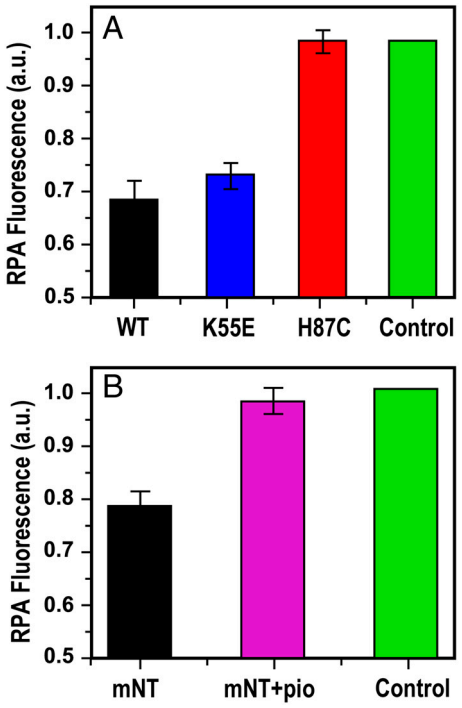

Fig. 5. Transfer of [2Fe-2S]/Fe from mNT's mutants to permeabilized HEK293 cells labeled with RPA. (*A*) RPA fluorescence was measured 20 min after the addition of 10 μM of WT mNT or mutants: WT mNT (black), K55E (blue), and H87C (red) bar, respectively. The green bar represents a fluorescence trace from control cells with no additions. Data are represented as mean ± standard error (SE). ($N = 17$). (*B*) The antidiabetic drug, pioglitazone, inhibits the Fe/Fe-S transfer from mNT to mitochondria in permeabilized HEK293 cells. Permeabilized cells loaded with RPA were examined by fluorescence microscopy as previously described. The data represent RPA levels 20 min after the addition of: 10 μM mNT (black bar), mNT (10 μM) preincubated with pioglitazone (100 μM), noted as mNT + pio, (purple bar), and a fluorescence trace from control cells with no additions (green bar). Data are represented as mean ± standard error (SE). The statistical differences between treatments were determined by paired *t* test at significance levels $p < 0.01$. ($N = 4$).

[2Fe-2S] proteins. Notably, do mNT proteins play a role in [2Fe-2S] cluster transfer along with the mitochondrial iron-sulfur cluster assembly (ISC) or cytosolic iron-sulfur cluster assembly (CIA) machinery (17, 42), as mNT's unique position on the outer mitochondrial membrane suggests it could be useful as a conduit between the cytosol and the mitochondria? Is mNT an [2Fe-2S]/Fe reservoir that provides clusters upon demand (6)? It is possible that mNT acts as a redox sensor and transfers its cluster only when in the oxidized state, such as when cells are stressed. It was long assumed that the TZD class of antidiabetes drugs acted only in a PPARγ-mediated fashion. Because pioglitazone inhibits

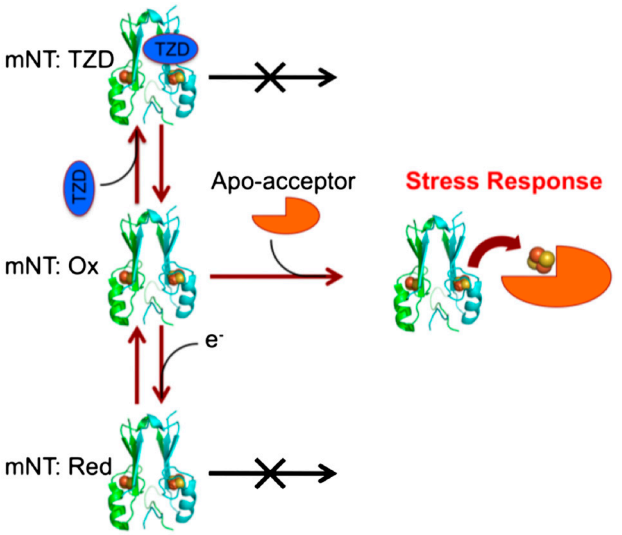

Fig. 6. Model describing a possible therapeutic mode of action for pioglitazone. Because the cytosol is normally highly reducing (39), we expect mNT to be predominantly in the reduced state. Changes to the cytosolic redox potential, which occur when cells are under oxidative stress (40), could induce transfer of mNT's [2Fe-2S] cluster. If not carefully regulated, this could lead to Fe overload stress, which is a problem in patients with type II diabetes (41). Pioglitazone, which shows a strong preferential binding to mNT in the oxidized state (8), may act to alleviate this stress.

this biochemical process it is clear that determining mNT's protein partners and a better understanding of how the protein–drug interaction relates to alleviating the negative effects of type II diabetes will be of great importance in the future.

Methods

All the materials used in this work were from best available commercial grade. The acetoxymethyl ester (AM) of calcein green (CalG) was obtained from Molecular Probes. The mitochondrial metal sensor red rhodamine B-[(1,10-phenanthrolin-5-yl) aminocarbonyl] benzyl ester (RPA) was obtained as described elsewhere (43, 44). Pioglitazone (purchased from Shanghai PI Chemicals Ltd.) was dissolved in 100% DMSO and diluted in test medium prior to use.

Expression and Purification of mNT Proteins and a-Fd. The human mNT cDNA encoding the cytoplasmic soluble (mNT) part of the protein (residues 33–108) was amplified by PCR and subcloned into a modified pET28-a(+) vector (Novagen) as described (36). The K55E and H87C mutants of mNT were generated by site-directed mutagenesis of the truncated mNT gene in the bacterial expression vector. The recombinant human mNT and mutant proteins were expressed in *Escherichia coli* BL21-RIL grown in LB supplemented with 30 μg/mL kanamycin and 34 μg/mL chloramphenicol. At an OD_{600} of 0.6, 0.75 mM $FeCl_3$ was added and cell growth proceeded for additional 18–24 h at 23 °C. From lysed cells, the mNT or mutant proteins were purified using Ni-agarose and size exclusion chromatography as described (30, 33, 36). Purification of a-Fd was performed as described previously (45). Protein concentrations were determined both by Bradford assay (46) and by spectroscopic methods using extinction coefficient at 280 nm of 9,400 $cm^{-1}\,M^{-1}$ for mNT and 9,100 $cm^{-1}\,M^{-1}$ for Fd.

UV-Vis Absorption Spectroscopy Transfer Kinetics and Decays. Absorption spectra were recorded at 350–600 nm (CARY, 300Bio), equipped with a temperature control apparatus set to 37 °C. Special attention was given to changes in absorbance at 458 nm (mNT's signature [2Fe-2S] absorbance peak) and at 423 nm (characteristic of the [2Fe-2S] cluster in Fd). The extent of cluster transfer was determined from the ratio $R = A^{423}/A^{458}$ as shown below:

$$\text{Reaction Progress} = (R_{\text{obs}} - R_{\text{initial}})/(R_{\text{final}} - R_{\text{initial}})$$

In the equation above, R_{obs} is the observed A^{423}/A^{458} ratio at a given time. R_{initial} is the initial A^{423}/A^{458} ratio at time 0, which is equal to 0.85, and R_{final} is the A^{423}/A^{458} ratio at long times when the reaction is considered complete and equal to 1.14. Data is normalized and fit to a single exponential rise. Initial transfer rates were determined by taking the tangent of the slope of the fit early into the transfer process (10 min) when concentrations of mNT and a-Fd were still close to their starting amounts. Kinetic measurements were performed using equimolar concentrations of mNT (WT and mutants) and a-Fd in the presence of 50 mM Tris pH 8.0, 100 mM NaCl, 5 mM DTT, and 5 mM EDTA, unless stated otherwise. The a-Fd and DTT were preincubated for 30 min prior to the start of the experiment. Decays were performed at 37 °C and determined by monitoring loss of the 458-nm peak with time. Data were then fit to a single exponential. Studies were performed using varying concentrations of mNT in 100 mM citrate 100 mM NaCl for pH < 6.5 and in 100 mM Bis-tris 100 mM NaCl for pH 6.5 and 7.0. As a check for possible buffer or salt effects on decay half-time, experiments at pH 6.0 and 6.5 were performed with both buffers and no significant differences in decay half-time were observed. The log-plotted pH-dependent slopes allowed for extrapolation of cluster decay times for pH 8.0, which were estimated to take nearly 10^5 min for WT and 10^6 minutes for the K55E and H87C mutants.

Native-PAGE [2Fe-2S] Cluster Transfer in Vitro Assay. WT mNT and mutants were incubated (in a rolling shaker) with a-Fd. Both mNT and a-Fd concentrations were 160 μM so that bands could be clearly visualized. The mNT and a-Fd were incubated under vigorous aeration in the presence of 2% β-mercaptoethanol, 5 mM DTT and 5 mM EDTA for the specified time lengths (2.5–60 min). β-mercaptoethanol was added to better keep disulfides reduced because the degree of aeration was higher in the gel assay than in the UV-Vis measurements. Transfer of the [2Fe-2S] cluster from mNT to a-Fd was then analyzed by native-PAGE (47) and checked for completion by UV-Vis spectroscopy.

Labeling of mNT [2Fe-2S] Cluster. $^{55}FeCl_3$ (PerkinElmer, Life Sciences Inc.) was diluted with 100 mM sodium citrate pH 8.0 to 1 μci and incubated with mNT at 1:1 ratio (final 2 mM sodium citrate pH 8.0) at 4 °C for a week in a rolling shaker. Following the incubation, mNT was concentrated by centrifugation (4,000 rpm at SS-34 rotor) using a microcon YM-10 (Millipore) filter and washed three times with large excess citrate buffer. Radioactivity was determined on Beckman LS2800 counter (Beckman) and protein labeling was analyzed by native-PAGE and revealed with a phosphor-imager (FujiFilm FLA-3000, Fujifilm Medical Systems).

Cell Culture. Human Embryonic Kidney cells (line HEK293) were grown at 37 °C in 5% CO_2 in Dulbecco's modified Eagle's medium (DMEM; Biological Industries) supplemented with 1% antibiotics (penicillin, streptomycin, and amphotericin), 1% glutamine, and 10% fetal calf serum. A day before experimentation, the cells were washed with PBS and then detached from plates with 1 ml trypsin-ethylene diamine tetraacetic acid. The cells were diluted to an optimal density of 1–2 million cells per plate (3-cm perforated plate with microscopic slides attached). The cells were further grown for additional 24 h and subjected to epifluorescence imaging on a Zeiss Axiovert 35 (Carl Zeiss) microscope attached to a Polychrome V image system (Till Photonics) (48).

Fluorescence Measurements. HEK293 cells were labeled for 15-min at 37 °C with 1 μM RPA and/or 0.1 μM CalG-AM in DMEM medium containing 10 mM HEPES buffer and supplemented with 10 μM desferrioxamine (DFO) to prevent quenching of the probe by contaminant iron from the medium. After washing with DMEM-HEPES medium and HEPES-buffered saline (HBS) buffer, the cells were permeabilized in HBS buffer pH 7.4 for 180 s with 25 μM digitonin (49). The permeabilized cells were washed with permeabilization buffer (100 mM KCl, 5 mM phosphate buffer, Eagle's MEM-amino acids mix diluted 1:500, 10 mM HEPES, 1 μM $CaCl_2$, 1 mM $MgSO_4$, pH 7.2) and taken to fluorescence microscopy measurements in permeabilization buffer containing 1 mM succinate. For CALG (λexc 480 nm; λ em 520 nm) (50, 51) and RPA (560 nm excitation-610 nm emission) (43, 44), as described elsewhere (48, 50, 51). DFO (1 μM) was present in all solutions during permeabilization and fluorescence measurements, to prevent RPA quenching by contaminant iron. After a 6-min baseline was recorded, 10–50 μM mNT (WT or mutants) was added (with 1 mM DTT) and changes in fluorescence were recorded for 20 min at 37 °C followed by addition of a permeant form of labile iron-FHQ (5 μM FHQ ([$FeCl_3$-8-hydroxyquinoline 1:1 complex) so as to attain maximal quenching. The sequence of fluorescence images acquired by microscopy were analyzed by the Image J program (National Institutes of Health) (52).

ACKNOWLEDGMENTS. We would like to thank Syed Ali for his assistance with the cluster transfer UV-Vis experiments. This work was supported by the Israel Science Foundation (ISF). ISF 863/09 awarded to R.N.; ISF 141/06 and a grant from the Canadian Friends of the Hebrew University awarded to Z.I.C.; ISF 214/08 and the European Union Grant FP7-Marie Curie 447 awarded to R.M.; the CMG Grant 2T32GM007240-29 awarded to A.R.C.; National Institutes of Health (NIH) grants GM41637 (M.L.P), NIH GM54038 and NIH DK54441 (to P.A.J.); and the Heme and Blood Proteins Training Grant 5T32DK007233-34 (J.A.Z.).

1. Colca JR, et al. (2004) Identification of a novel mitochondrial protein ("mitoNEET") cross-linked specifically by a thiazolidinedione photoprobe. *Am J Physiol Endocrinol Metab* 286:E252–260.
2. Colca JR, Kletzien RF (2006) What has prevented the expansion of insulin sensitisers? *Expert Opin Investig Drugs* 15:205–210.
3. Hofmann CA, Colca JR (1992) New oral thiazolidinedione antidiabetic agents act as insulin sensitizers. *Diabetes Care* 8:1075–1078.
4. Cavender MA, Nicholls SJ, Lincoff AM (2010) Strategies for the development of new PPAR agonists in diabetes. *J Cardiovasc Risk* 17:s32–s37.
5. Schmidt MV, Brune B, von Knethen A (2010) The nuclear hormone receptor PPAR? as a therapeutic target in major diseases. *ScientificWorldJournal* 10:2181–2197.
6. Paddock ML, et al. (2007) MitoNEET is a uniquely folded 2Fe-2S outer mitochondrial membrane protein stabilized by pioglitazone. *Proc Natl Acad Sci USA* 104: 14342–14347.
7. Wiley SE, et al. (2007) The outer mitochondrial membrane protein mitoNEET contains a novel redox-active 2Fe-2S cluster. *J Biol Chem* 282:23745–23749.
8. Bak DW, Zuris JA, Paddock ML, Jennings PA, Elliott SJ (2009) Redox characterization of the FeS protein mitoNEET and impact of thiazolidinedione drug binding. *Biochemistry* 48:10193–10195.
9. Conlan AR, et al. (2009) Crystal structure of Miner1: The redox-active 2Fe-2S protein causative in Wolfram syndrome 2. *J Mol Biol* 392:143–153.
10. Chang NC, Nguyen M, Germain M, Shore GC (2009) Antagonism of beclin 1-dependent autophagy by BCL-2 at the endoplasmic reticulum requires NAF-1. *EMBO J* 29:606–618.
11. Chen YF, et al. (2009) Cisd2 deficiency drives premature aging and causes mitochondria-mediated defects in mice. *Gene Dev* 23:1183–1194.
12. Amr S, et al. (2007) A homozygous mutation in a novel zinc-finger protein, ERIS, is responsible for Wolfram syndrome 2. *Am J Hum Genet* 81:673–683.

13. Lin J, Zhou T, Ye K, Wang J (2007) Crystal structure of human mitoNEET reveals distinct groups of iron-sulfur proteins. *Proc Natl Acad Sci USA* 104:14640–14645.
14. Hou X, et al. (2007) Crystallographic studies of human mitoNEET. *J Biol Chem* 282:33242–33246.
15. Johnson DC, Dean DR, Smith AD, Johnson MK (2005) Structure, function, and formation of biological iron sulfur clusters. *Annu Rev Biochem* 74:247–281.
16. Lill R, Mühlenhoff U (2008) Maturation of iron-sulfur proteins in eukaryotes: Mechanisms, connected processes, and diseases. *Annu Rev Biochem* 77:669–700.
17. Lill R (2009) Function and biogenesis of iron-sulphur proteins. *Nature* 460:831–838.
18. Rouault TA, Tong WH (2008) Iron-sulfur cluster biogenesis and human disease. *Trends Genet* 24:398–407.
19. Adinolfi S, et al. (2009) Bacterial frataxin CyaY is the gatekeeper of iron-sulfur cluster formation catalyzed by IscS. *Nat Struct Mol Biol* 16:390–396.
20. Napier I, Ponka P, Richardson DR (2005) Iron trafficking in the mitochondrion: novel pathways revealed by disease. *Blood* 105:1867–1874.
21. Camaschella C, et al. (2007) The human counterpart of zebrafish shiraz shows sideroblastic-like microcytic anemia and iron overload. *Blood* 110:1353–1358.
22. Sohn Y-S, Breuer W, Munnich A, Cabantchik ZI (2008) Redistribution of accumulated cell iron: A modality of chelation with therapeutic implications. *Blood* 111:1690–1699.
23. Hausmann A, Samans B, Lill R, Mühlenhoff U (2008) Cellular and mitochondrial remodeling upon defects in iron-sulfur protein biogenesis. *J Biol Chem* 283:8318–8330.
24. Hentze MW, Muckenthaler MU, Andrews NC (2004) Balancing acts: Molecular control of mammalian iron metabolism. *Cell* 117:285–297.
25. Hansen TM, Nagley P (2003) AIF: A multifunctional cog in the life and death machine. *Sci STKE* 193:PE31.
26. Cusimano EM, Knight AR, Slusser JG, Clancy RL, Pierce JD (2009) Mitochondria: The hemi of the cell. *Adv Emerg Nurs J* 31:54–62.
27. Abdul-Ghani M, DeFronzo R (2008) Mitochondrial dysfunction, insulin resistance, and type 2 diabetes mellitus. *Curr Diab Rep* 8:173–178.
28. Lowell BB, Shulman GI (2005) Mitochondrial dysfunction and type 2 diabetes. *Science* 307:384–387.
29. Saxena R, et al. (2006) Comprehensive association testing of common mitochondrial DNA variation in metabolic disease. *Am J Hum Genet* 79:54–61.
30. Baxter EL, Jennings PA, Onuchic JN (2011) Interdomain communication revealed in the diabetes drug target mitoNEET. *Proc Natl Acad Sci USA* 108:5266–5271.
31. Zuris JA, et al. (2010) Engineering the redox potential over a wide range within a new class of FeS proteins. *J Am Chem Soc* 132:13120–13122.
32. Dicus MM, et al. (2010) Binding of histidine in the (Cys)3(His)1-coordinated [2Fe-2S] cluster of human mitoNEET. *J Am Chem Soc* 132:2037–2049.
33. Conlan AR, et al. (2011) Mutation of the His ligand in mitoNEET stabilizes the 2Fe-2S cluster despite conformational heterogeneity in the ligand environment. *Acta Crystallogr D Biol Crystallogr* 67:516–523.
34. Tirrell TF, et al. (2009) Resonance Raman Studies of the (His)(Cys)3 2Fe-2S cluster of mitoNEET: Comparison to the (Cys)4 mutant and implications of the effects of pH on the labile metal center. *Biochemistry* 48:4747–4752.
35. Wu SP, Cowan JA (2003) Iron-sulfur cluster biosynthesis. A comparative kinetic analysis of native and Cys-substituted ISA-mediated [2Fe-2S]2+ cluster transfer to an apoferredoxin target. *Biochemistry* 42:5784–5791.
36. Conlan AR, et al. (2009) The novel 2Fe-2S outer mitochondrial protein mitoNEET displays conformational flexibility in its N-terminal cytoplasmic tethering domain. *Acta Crystallogr Sect F Struct Biol Cryst Commun* 65:654–659.
37. Hou X, et al. (2007) Crystallographic studies of human mitoNEET. *J Biol Chem* 282:33242–33246.
38. Shimomura Y, Wada K, Fukuyama K, Takahashi Y (2008) The asymmetric trimeric architecture of [2Fe-2S] IscU: Implications for its scaffolding during iron-sulfur cluster biosynthesis. *J Mol Biol* 383:133–143.
39. Martinovich GG, Cherenkevich SN, Sauer H (2005) Intracellular redox state: Towards quantitative description. *Eur Biophys J* 34:937–942.
40. Schwarzer C, et al. (2008) Oxidative stress caused by pyocyanin impairs CFTR Cl- transport in human bronchial epithelial cells. *Free Radical Biol Med* 45:1653–1662.
41. Black PH (2003) The inflammatory response is an integral part of the stress response: Implications for atherosclerosis, insulin resistance, type II diabetes and metabolic syndrome X. *Brain Behav Immun* 17:350–364.
42. Netz DJ, Pierik AJ, Stumpfig M, Muhlenhoff U, Lill R (2007) The Cfd1-Nbp35 complex acts as a scaffold for iron-sulfur protein assembly in the yeast cytosol. *Nat Chem Biol* 3:278–286.
43. Petrat F, et al. (2002) Selective determination of mitochondrial chelatable iron in viable cells with a new fluorescent sensor. *Biochem J* 362:137–147.
44. Rauen U, et al. (2003) Cold-induced apoptosis of hepatocytes: mitochondrial permeability transition triggered by nonmitochondrial chelatable iron. *Free Radical Biol Med* 35:1664–1678.
45. Fish A, Danieli T, Ohad I, Nechushtai R, Livnah O (2005) Structural basis for the thermostability of ferredoxin from the cyanobacterium Mastigocladus laminosus. *J Mol Biol* 350:599–608.
46. Bradford MM (1976) A rapid and sensitive method for the quantitation of microgram quantities of protein utilizing the principle of protein-dye binding. *Anal Biochem* 72:248–254.
47. Peter GF, Thornber JP (1991) Biochemical composition and organization of higher plant photosystem II light-harvesting pigment-proteins. *J Biol Chem* 266:16745–16754.
48. Glickstein H, Ben El R, Shvartsman M, Cabantchik ZI (2005) Intracellular labile iron pools as direct targets of iron chelators: A fluorescence study of chelator action in living cells. *Blood* 106:3242–3250.
49. Nishikawa M, Nojima S, Akiyama T, Sankawa U, Inoue K (1984) Interaction of digitonin and its analogs with membrane cholesterol. *J Biochem* 96:1231–1239.
50. Glickstein H, et al. (2006) Action of chelators in iron-loaded cardiac cells: Accessibility to intracellular labile iron and functional consequences. *Blood* 108:3195–3203.
51. Espósito BP, Epsztejn S, Breuer W, Cabantchik ZI (2002) A review of fluorescence methods for assessing labile iron in cells and biological fluids. *Anal Biochem* 304:1–18.
52. Abramoff MD, Magalhaes M, Ram SJ (2004) Image processing with ImageJ. *Biophoton Int* 11:36–42.